published by Ural Federal University
eISSN 2411-1414
chimicatechnoacta.ru

REVIEW
2025, vol. 12(1), No. 12111
DOI: 10.15826/chimtech.2025.12.1.11

Doping effects on the structure, transport properties, and chemical stability of $LaInO_3$ perovskite: A review

Anastasia Egorova [ab*], Ksenia Belova [a], Irina Animitsa [a]

a: Institute of Natural Sciences and Mathematics, Ural Federal University,
Ekaterinburg 620009, Russia
b: Institute of Solid State Chemistry of the Ural Branch of the Russian Academy of Sciences,
Ekaterinburg 620041, Russia
* Corresponding author: OAV-hn@yandex.ru

Abstract

The desire to use novel functional materials in electrochemical devices stimulates significant research in materials science. Complex oxides with a perovskite-like structure occupy a large niche among such materials. Solid solutions based on $LaInO_3$ exhibit promising ionic conductor properties (O^{2-}, H^+) combined with high chemical stability. This review presents a comprehensive analysis of the physicochemical properties of doped $LaInO_3$ materials. The structure and hydration processes of parent and doped compounds are discussed. The transport properties data were collected and summarized. Both the pure and the doped materials exhibit mixed ion-hole conductivity in dry air. All solid solutions based on $LaInO_3$ are capable of reversible incorporation of water vapor due to their effective oxygen vacancy size close to r_{an}~1.4 Å. Under elevated humidity conditions, proton transfer is observed in the samples. The data indicates a correlation between an increase in free cell volume and an increase in ionic conductivity. The results on chemical stability and TEC for the pure and doped materials are analyzed. The strategy for selecting dopant cations is shown. The presented data show the potential for applications of $LaInO_3$-based materials in electrolyte membranes for solid oxide fuel cells, pumps and sensors.

Key findings

- Pure $LaInO_3$ and the majority of solid solutions are characterized by a perovskite structure with orthorhombic symmetry.
- Doped $LaInO_3$ materials are able to dissociatively incorporate water vapor at temperatures below 500 °C, with the experimental degree of hydration reaching 90% of the theoretical value.
- A significant enhancement in electrical conductivity (~3 orders of magnitude) in comparison to pure $LaInO_3$ results from the A sublattice substitution.
- A general tendency is towards an increase in electrical conductivity accompanied by an increase in the free volume cell.
- The proton conductivity of doped $LaInO_3$ materials is comparable to the data for the known protonic conductors $LaScO_3$ and $BaZr_{0.8}Y_{0.2}O_{3-\delta}$.

© 2024, the Authors. This article is published in open access under the terms and conditions of the Creative Commons Attribution (CC BY) license (http://creativecommons.org/licenses/by/4.0/).

Accompanying information

Article history
Received: 08.11.24
Revised: 09.12.24
Accepted: 17.12.24
Available online: 23.12.24

Keywords
perovskite; lanthanum indate; free volume cell; hydration; proton conductivity; chemical stability

Funding
The work was carried out in accordance with the state assignment for the Institute of Solid State Chemistry of the Ural Branch of the Russian Academy of Sciences, theme No. 124061300025-8.

Supplementary information
Supplementary materials: READ
Transparent peer review: READ

Sustainable Development Goals
7 AFFORDABLE AND CLEAN ENERGY

1. Introduction

The latest developments in the electric power sector indicate a growing interest in solid oxide fuel cells (SOFCs) as a potential alternative to conventional energy sources [1–4]. SOFCs operating in an intermediate temperature range (500–700 °C) demonstrate the greatest potential, because their electrolytic membranes can be used as proton conductors based on complex oxides [5–7]. The main task of the materials science is to identify a technologically viable, chemically stable, and cost-effective solid electrolyte with high ionic conductivity.

In the context of proton conductors, complex oxides with perovskite structures are a subject of extensive research [7–9]. The presence of hydrogen in the structure of complex oxides is ensured by equilibrium with the H_2O/H_2-

containing atmosphere, which is described as a process of dissociative incorporation of water vapor [10, 11]. Materials based on doped perovskites ABO_3 with alkaline earth cations, such as $BaCeO_3$ and $BaZrO_3$, are among the most extensively studied materials due to their best proton conductivity [9,12,13]. A notable limitation of $BaZrO_3$-based materials is their considerable grain boundary resistance [14–16]. Furthermore, $BaCeO_3$-based materials exhibit low chemical stability towards CO_2 and water vapor, [17–20], which is usually associated with the presence of an alkaline earth element.

Consequently, in recent years, the search for new strategies in achieving a compromise between chemical stability and high ionic conductivity has become a relevant field of investigations [21, 22]. A promising way of research is the development of new materials that do not contain an alkaline earth component in their chemical formula – "*alkaline earth elements-free strategy*" [23–25]. In this regard, the perovskite-like compounds demonstrate remarkable prospects, since their structure is capable of adapting various charge combinations of elements [26], for example, the perovskites of the composition $A^{3+}B^{3+}O_3$ that do not contain alkaline earth elements. Among the perovskites of the composition $A^{3+}B^{3+}O_3$, the compounds containing lanthanum exhibit considerable potential, as La^{3+} has a large ionic radius [27], as a consequence a highly symmetrical crystalline lattice [28], which is a favorable factor for high ionic conductivities. The number of acceptor-doped lanthanum-containing perovskites, $LaB^{3+}O_3$ (B^{3+}=Al, Ga, Sc, In, Yb, Y), display a high level of ion (O^{2-} or H^+) transport [29–31]. The doped perovskites $LaGaO_3$ [32, 33] and $LaAlO_3$ [30, 34] are described as oxygen-ion conductors, whereas doped $LaYO_3$ [35, 36] and $LaYbO_3$ [37, 38] can exhibit predominantly proton transport in wet atmospheres. The doped scandates $LaScO_3$ [39–42] and indates $LaInO_3$ [43–45], are capable of exhibiting *co-ionic* transport depending on the conditions.

The doped $LaScO_3$ materials have been the subject of more extensive study due to their superior proton conductivity. The substituted $LaInO_3$ indates have not yet been extensively studied with regard to their potential as proton conductors. However, $LaInO_3$-based materials are of significant interest due to their chemical stability and lower cost in comparison with $LaScO_3$ materials. Moreover, the results of conductivity studies are contradictory and unsystematic. In this article we have systematized the data on the structure of doped $LaInO_3$ and its influence on electrical properties.

2. Structural features of pure and doped $LaInO_3$

The structure of lanthanum indate ($LaInO_3$) has been investigated since as early as the mid-twentieth century [46, 47]. Subsequently, the structure of $LaInO_3$ was subjected to comprehensive analysis in [48–50]. The orthorhombic perovskite $LaInO_3$ (sp. gr. *Pnma* [49,51] or *Pbnm* [52,53]) is composed of chains of $[InO_6]$ octahedra, as illustrated in Figure 1. The ionic radius of La^{3+} (for XII-fold coordination) and In^{3+} (for VI-fold coordination) is 1.36 and 0.80 Å, respectively [27]. A discrepancy between the In–O and La–O layers can result in lattice distortion, such as the tilting of the $[InO_6]$ octahedra. This distortion can lead to an In–O1–In bond angle that is less than 180° [51]. The distortion is well visualized when the structure is plotted as a network of $[InO_6]$ octahedra, which are commonly used to describe ideal cubic perovskite (Figure 1).

The lanthanum indate system exhibits two distinct crystallographic orientations of the oxygen atom. These are observed as two apical (O1) positions located at opposing corners of the octahedron along the *b*-axis and four equatorial (O2) positions within the *a*–*c* plane of the octahedron. The existence of multiple O–O distances is of significant importance with regard to the migration of hydrogen, as the reduction in symmetry can impede proton transport as a result of the concerted movement of oxygen required for the jump [54].

The orthorhombic structure of lanthanum indate remains stable even when doped, although the structure accommodates small concentrations of dopants. When lanthanum is replaced by other rare earth elements, for example Sm^{3+}[55, 56], Nd^{3+} [57], Dy^{3+} [51], Tb^{3+} or Eu^{3+} [58, 59], the dopant concentration reaches 5–10 mol%. For instance, gallium is able to substitute lanthanum in these positions up to 20 mol% [60]. The available structural data for the various doped phases based on $LaInO_3$ (*LIO*) are presented in Table S1 (Supplementary). Table S1 includes the unit cell parameters (*abc*), volume cell ($V = a \cdot b \cdot c$), unit cell volume divided by the formula unit ($\tilde{V}_{cell} = a \cdot b \cdot c/Z$), free volume cell ($V_{free}$), and anion radius ($r_{\text{an}}$), discussed in section 3.

The "*free volume cell*" (V_{free}) parameter was first proposed in the 1990s to explain alterations in the transport properties of materials. This approach has since been supported by numerous reviews [61–64]. The free cell volume parameter is defined as the volume of the cell that is not occupied by all the constituent atoms, according to:

$$V_{free} = \tilde{V}_{cell} - \sum m_i \left(\frac{4}{3}\right) \pi r_i^3, \tag{1}$$

where $\tilde{V}_{cell}$ is the unit cell volume divided by the number of formula units (Z = 4), m_i is index of the atom in the oxide, and r_i is ionic radius of the i-th element in the oxide.

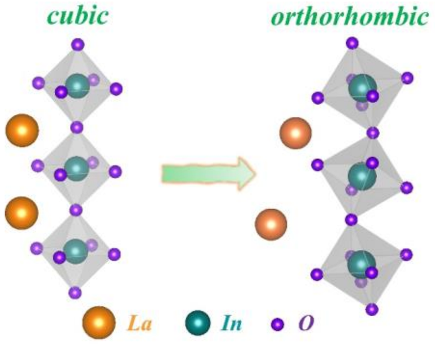

Figure 1 Transformation from a cubic symmetry to an orthorhombic structure.

An ideal cubic perovskite structure with a space-filling ion is presented in Figure 2a. The corner of the structure was removed. The cutting plane projection is presented in Figure 2b. The free volume is shown in yellow in Figure 2.

A correlation is observed between the enhanced ionic conductivity and the increased free volume of the unit cell in doped $LaInO_3$ materials, which are discussed in detail in Section 4.3.

The most common doping strategy in lanthanum-containing perovskites is the substitution with an alkaline earth elements [31, 54, 61, 65, 66]. In the $LaInO_3$ matrix, the possibility of substituting both the lanthanum and indium sites was investigated. Figure 3 shows the dissolution energy of alkaline earth metals in $LaInO_3$ in La^{3+} and In^{3+} sites [48]. The lowest values of the dissolution energy in the *A-sites* are observed for strontium and calcium, which can be attributed to the close ionic radii of the host and dopant cations for the XII-fold coordination [27].

The $La_{1-x}Ca_xInO_{3-\delta}$ solid solution [43, 67] was synthesized by replacing lanthanum with calcium. The solubility limit in this system is $x = 0.10$. As the concentration of Ca^{2+} is increased up to 10 mol%, the lattice volume displayed a corresponding increase. An increase in the calcium content (15–20 mol%) results in the formation of the second phase ($CaIn_2O_4$).

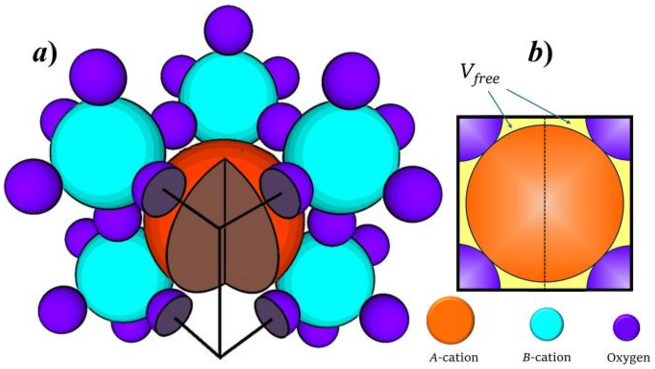

Figure 2 An ideal cubic perovskite structure as space-filing ion model with a cut corner (a); A section view of the unit cell fragment (b); the ions are shown in the corresponding color; the border of the unit cell is represented by the black line, and the free volume of the cell as space not occupied by any of the constituent ions is shown in yellow.

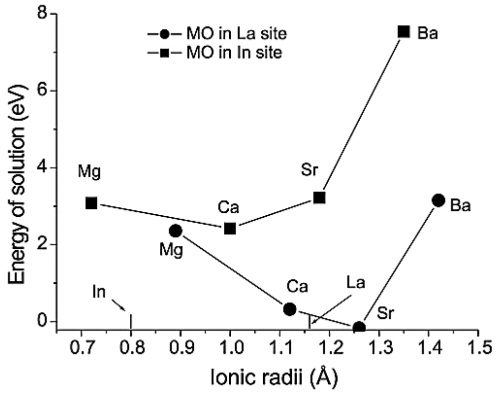

Figure 3 The solution energy of alkaline earth metals in $LaInO_3$. Reproduced from ref. [48]. Copyright 2002, Elsevier.

A similar trend was observed in the case of the $La_{1-x}Sr_xInO_{3-\delta}$ solid solution [52, 68, 69]. As the Sr^{2+} content increases from 0 to 10 mol%, the orthorhombic structure is distorted, and the unit cell volume increases; with a further increase in x up to 0.2, the cell volume remains unchanged. Furthermore, an impurity phase of the composition $SrIn_2O_4$ is formed. Consequently, the maximum Sr^{2+} content in $LaInO_3$ was determined to be 10 mol% [52]. The introduction of a dopant with a concentration below 0.1 has not been explored in the existing literature.

As can be seen from Figure 3 the highest solution energies are observed for magnesium and barium dopants, which can be attributed to their size characteristics. In the case of Mg^{2+}, no ionic radius values are provided for the XII-fold coordination [27], and the question arises as to whether it can be considered a dopant of the A-sublattice. Conversely, the ionic radius of barium (1.61 Å for the XII-fold coordination) is significantly larger than that of lanthanum (1.36 Å for the XII-fold coordination) [27]. While barium is indeed capable of replacing lanthanum in such structures, its solubility limit does not exceed 5 mol% [66, 70].

It is important to note that the $La_{1-x}Ba_xInO_{3-\delta}$ complex oxide exhibits a different crystal symmetry when the Ba content is varied [66, 70–74]. In a solid solution with $x \leq 0.05$, the system exhibits orthorhombic symmetry. A higher dopant concentration ($x = 0.1–0.3$) leads to the formation of a mixture of cubic and orthorhombic phases. As the fraction of Ba^{2+} ions increases, the tolerance factor t approaches 1 [70], and the formation of the cubic phase becomes the predominant process. Ultimately, the material crystallizes in a cubic monophase when the concentration of barium is high ($x = 0.4–0.70$) and in a tetragonal phase when $x = 0.8$ [66, 71]. It was demonstrated that a cubic modification could be obtained through the simultaneous doping of barium and strontium at concentrations of 30 mol% and 20 mol%, respectively [75]. Except for these works, no other studies confirmed the formation of structures with cubic symmetry. But, similarly, alteration of the crystal structure was observed in Ba-doped lanthanum scandate materials [76, 77]. As the ionic radii of indium (0.800 Å, for the VI-fold coordination) and scandium (0.745 Å, for the VI-fold coordination) are similar [27], analogous trends in the structural features of lanthanum indate and scandate may be anticipated. For example, a cubic modification can be achieved for $LaScO_3$ for the substitution by Sr^{2+} ions at an elevated dopant level ($x \leq 0.35$) [78].

The quasichemical reaction of dissolution of the alkaline earth metal oxide *Me*O in the lanthanum sites with formation of the acceptor defects Me'_{La} can be written as follows:

$$2\mathrm{MeO} \xrightarrow{\mathrm{La_2O_3}} 2\mathrm{Me}'_{\mathrm{La}} + \mathrm{V}_{\mathrm{O}}^{\bullet\bullet} + 2\mathrm{O}_{\mathrm{O}}^{\mathrm{x}} \qquad (2)$$

where $\mathrm{Me}'_{\mathrm{La}}$ is the dopant on lanthanum site, $\mathrm{V}_{\mathrm{O}}^{\bullet\bullet}$ is the oxygen vacancy, and $\mathrm{O}_{\mathrm{o}}^{\mathrm{x}}$ is the oxygen atom in the regular

DOI: 10.15826/chimtech.2025.12.1.11

position. Most studies on $LaInO_3$ have focused on the effects of substitutions in the *A*-sublattice. However, there are some studies on the effect of doping in the B-sublattice on the physico-chemical properties. The solubility limits when replacing the In^{3+} cation, for instance, with polyvalent ions Mn^{3+} [53, 57], Cr^{3+}[57, 79], Sb^{3+} [53] or Sn^{4+} [80] did not exceed 3–5 mol%. The introduction of a heterovalent dopant of Zn^{2+} into In^{3+} was first reported in [80] and was subsequently subjected to comprehensive investigation in work [45], wherein a dopant concentration of 5–7 mol% was established. The introduction of zinc into the indium sites in a 1:1 ratio was investigated in the work [81]; however, this substitution did not lead to the stabilization of the cubic structure. This can be explained by the close ionic radii of indium and zinc. The substitution for Zr^{4+} as a donor was investigated in [44], wherein the concentration of dopant was found to reach 10 mol%.

The B-cation can be replaced by any alkaline earth metal, as shown in Figure 3 [48]. It was observed that the solution energy of CaO in the In^{3+}-position exhibited the lowest value, although such substitution was not described in the literature. Typically, indium substitutions were implemented as joint doping involving both the A- and B-sublattices.

The effects of co-doping strategy on $LaInO_3$ structure were investigated in the works [44, 52, 74, 82]. The primary objective of these studies was to investigate strontium-containing phases. The Sr^{2+} ionic radius is slightly larger than that of the La^{3+} host atom for the XII-fold coordination [27], resulting in an expansion of the crystal lattice of the phases. This expansion may contribute to the widening of the region of homogeneity of systems with co-doping cations, as it was observed for Mg^{2+}- and Ca^{2+} co-dopants in the works [82, 83]. Consequently, a high dopant concentration results in an increase in oxygen vacancy concentration, thereby enhancing the functional characteristics of the material.

The co-doped solid solution with Ca^{2+} in La-sites has not been described in literature. Similarly, there is a scarcity of information regarding barium-containing co-doped solid solutions with orthorhombic symmetry. Although the investigations [74, 84] were devoted to co-doped cubic phases with a Ba^{2+} concentration of around 40–50 mol%, this was due to their high proton conductivity.

Consequently, the structural characteristics of pure and doped $LaInO_3$ materials can be summarized as follows:

i. The solubility limit for dopants in both A- and B-sublattices was found to be narrow, with a maximum of 10 mol% for the majority of dopants.
ii. The undoped phase and most solid solutions based on lanthanum indate crystallize in a perovskite structure with orthorhombic symmetry. This is applicable to dopants with ionic radii that are close to those of the host cations and to solid solutions with narrow homogeneity regions (i.e. when *x* is no more than 10–20 mol%).
iii. The doping of materials with a large cation, either Ba^{2+} or Sr^{2+}, at concentrations that are relatively high ($x \geq 0.4$) can result in the stabilization of cubic symmetry.
iv. The lattice parameters change in accordance with the radius of the introduced metals.

3. Hydration processes

Pure lanthanum indate cannot incorporate water due to the complete oxygen sublattice [45, 48]. Doped $LaInO_3$ materials are capable of dissociative incorporation of water vapor from the gas phase at temperatures below 500 °C [29, 48, 85]. In a complex oxide with impurity disordering, the interaction with water molecules in the gas phase results in the filling of oxygen vacancies with oxygen from the water molecule. A quasi-chemical approach can be employed to describe the process of oxygen vacancy filling during dissociative water molecule incorporation into the structure of a complex oxide. The reaction can be written by the Kröger–Vink notation as follows [86]:

$$V_O^{\bullet\bullet} + O_o^x + H_2O \Leftrightarrow 2OH_o^{\bullet} \quad (3)$$

where $OH_o^{\bullet}$ is the hydroxyl group in the oxygen sublattice.

In accordance with the quasi-chemical reaction of filling oxygen vacancies with oxygen from water molecules, it is possible to calculate the value of the maximum water uptake, or the theoretical limit of hydration of compound. Since the dopant concentration is relatively low (less than 10 mol%), the theoretical hydration limit is also small. The experimental values of the degree of hydration for solid solutions reach 88–90% of the theoretical value [29, 45, 84]. The theoretical hydration limit of the complex oxide has not been reached, which can be explained by the following factors:

- The oxygen vacancies are not equivalent at the apical and equatorial oxygen positions in the crystal lattice, which makes them difficult to access.
- Doping by acceptor impurities and the formation of negatively charged defects A'_{La} or B'_{In} leads to their interaction with $V_O^{\bullet\bullet}$ oxygen vacancies, which makes it impossible for oxygen vacancies to interact with water [87, 88].

An alternative approach to the hydration processes can be taken from a crystalochemical point of view. The hydration process of complex oxides is accompanied by the introduction of water molecules (that is OH^--groups) into the structure. Consequently, this process requires sufficient space for the placement of additional O^{2-} atoms (or OH^--groups). In order to estimate the available space within the structure, one may apply the "*effective vacancy size*" strategy as developed in the works [89–93]. In this approach, the primary calculation parameters are the effective vacancy of oxygen size (r_V) and the anion radius (r_{an}). The value of the effective radius of a vacancy of oxygen is related to the radius of the anion by the following expression [92]:

$$r_{\mathrm{an}} = \frac{3-0.5x-0.5y}{3} r_{\mathrm{O}} + \frac{0.5x+0.5y}{3} r_{\mathrm{V}} \qquad (4)$$

where r_{O} is the ionic radius of oxygen (1.4 Å), r_{an} is the total anion radius, which denotes the average radius of all oxygen sites, including both occupied and vacant sites, and x, y are the dopant concentrations.

It was found that doped aluminates and gallates $\mathrm{LaB^{3+}O_3}$ exhibit low r_{V} values and that these phases do not exhibit proton transport. In contrast, proton-conducting doped scandates and indates display elevated r_{V} values [45, 92]. It is evident that there is a limit in the values of r_{V} below which the $\mathrm{OH^-}$-groups are not incorporated into the lattice. It seems reasonable to assume that this boundary is determined by the size r_{V} = 1.35 Å, which is consistent with the size of the $\mathrm{OH^-}$-group r_{OH} = 1.35 (IV) – 1.37 (VI) Å [27]. Since the calculated parameter r_{V} depends on the size of the oxygen ion, this parameter can be used as a criterion for the ability to hydrate for the phases with different cations in the A- and/or B-sublattices. The value of anion radius (r_{an}) for doped $\mathrm{LaInO_3}$ materials varies depending on the nature of the cations and can be calculated based on the structural data available and included in Table S1. If the values r_{an} are greater than 1.4 Å then there is enough space to place $\mathrm{OH^-}$ groups.

The hydration processes of doped $\mathrm{LaInO_3}$ phases were investigated in comparison with a series of other doped $\mathrm{LaB^{3+}O_{3-\delta}}$ systems ($\mathrm{B^{3+}}$ = Al, Sc, In, Yb, Y) [28–30]. The hydration processes in these materials exhibit non-monotonic behaviour. The substituted aluminites and gallates are unable to undergo significant hydration. The scandates and indates display a high hydration level, reaching up to 90% of the theoretical maximum. Nevertheless, upon analysis of the data from ytterbates and ytrates, it was found that the hydration limit is reached at 10% of the theoretical level.

The possibility of incorporation of water is directly correlated with the potential of the compound to exhibit proton conductivity.

4. Transport properties

4.1. Undoped perovskite $\mathrm{LaInO_3}$

The band structure of the $\mathrm{LaInO_3}$ perovskite is shown in Figure S1. Pure lanthanum indate is an emerging wide bandgap semiconductor with a bandgap of ~5.0 eV [49, 94]. The electrical properties of $\mathrm{LaInO_3}$ were initially investigated in 1967 by D. Rogers [95]. Subsequently, the electrical conductivity was subjected to comprehensive analysis [44, 66, 96], which was complemented by theoretical calculations [72]. However, there is no convergence in data regarding the electrical properties of the $\mathrm{LaInO_3}$ phase. Figures S2–S4 reproduce the original temperature dependencies of total conductivity from Ref. [43, 52, 66]. A decrease in conductivity is observed with increasing temperature for all curves, which is a typical behaviour of semiconductor materials. The conductivity dependences (see Figures S3–S4) exhibit inflections in the low-conducting area at approximately 300 °C, which is not discussed in detail in works [52, 66]. The plot log (σ) vs 1000/T for the $\mathrm{LaInO_3}$ phase, measured in the works [43–45, 80, 97], is shown in Figure 4.

The Figure 4 illustrates a significant data scatter, although most of the temperature-dependencies of conductivities (lines ***1***, ***2***, ***3***, and ***4***) are within half an order of magnitude. It is evident that dependence ***5*** is overestimated.

The conditions for the preparation of $\mathrm{LaInO_3}$ ceramics and the conductivity data are summarized in Table 1.

In general, the sintering conditions of the ceramic samples were similar, although the conductivity differences were significant. It should be said that the data for a single crystal are presented by dependence ***1*** in the Figure 4, which is probably the most reliable conductivity data set.

The conductivity of pure $\mathrm{LaInO_3}$ was examined as a function of the partial pressure of oxygen in works [30, 45, 80]. The ionic transport numbers calculated for the *LIO* sample were approximately 0.8 [45] over the entire temperature range studied, indicating that the $\mathrm{LaInO_3}$ sample is a mixed (ionic-electronic) conductor with a high share of ionic conductivity (80 %) [45, 48]. The humidity change did not affect the conductivity.

The migration of oxygen ions in the $\mathrm{LaInO_3}$ structure was investigated using molecular dynamics methods [72]. Figure 5 illustrates the octahedron $[\mathrm{InO_6}]$, demonstrating that the migration of oxygen ions does not occur in a linear trajectory between two adjacent oxygen atoms, but rather in a curved trajectory.

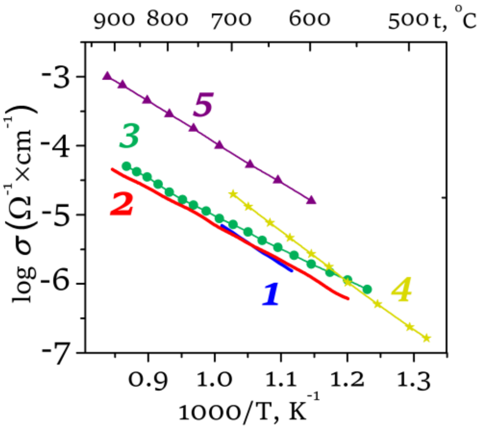

Figure 4 The temperature dependencies of electrical conductivity for $\mathrm{LaInO_3}$: ***1*** – [97], ***2*** – [80], ***3*** – [45], ***4*** – [43], ***5*** – [44].

Table 1 Synthesis conditions of $\mathrm{LaInO_3}$ ceramic materials.

$\mathrm{LaInO_3}$ [Ref.]	ρ_{relat} (%)	Sintering conditions T (°C)	time (h)	σ (S/cm) 650 °C
1 [97]	–	–	–	$2.5\cdot10^{-6}$
2 [80]	–	1400	2	$2.7\cdot10^{-6}$
3 [45]	97	1450	24	$3.9\cdot10^{-6}$
4 [43]	95	1400	12	$7.8\cdot10^{-6}$
5 [44]	–	1450	12	$3.8\cdot10^{-5}$

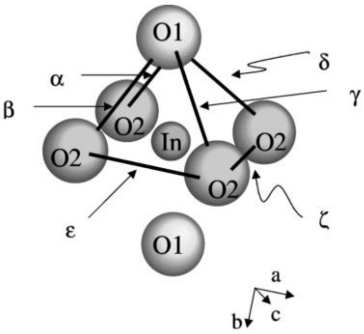

Figure 5 A distorted octahedron [InO_6] with the In in the center and six oxygen atoms in the corners; The symbols α, β, γ, δ, ε, ζ indicate the trajectory of the jump. Reproduced from ref. [48]. Copyright 2002, Elsevier.

The different O–O and In–O distances observed in the $LaInO_3$ structure, especially at the apical (O1) and equatorial (O2) oxygen positions, result in changes in the migration activation energy values. The oxygen atom O1 has the possibility to undergo four distinct types of atomic transitions. While some of these pathways exhibit similar lengths, they possess distinct activation energies. Most of the migration process from O1 entails migrating to the nearest O2. The migration of the O2 atom through the *a*-*c* plane can occur in two distinct pathways. Considering the interconnectivity of the two pathways, they must traverse each other. Furthermore, at elevated temperatures, transitions may occur between the O1 positions of neighboring octahedra. All calculated activation energy values values were within the range of 0.70–0.84 eV [48].

4.2. Electrical properties of mono-doped $LaInO_3$ materials

The electrical properties of pure $LaInO_3$ can be enhanced through the introduction of acceptor dopant in the *A*-site. The effect of doping with alkaline earth metals (10 mol.%) on electrical conductivity (Figure S2) was considered by He et al. [52]. The nature of the dopant proves to be a significant factor influencing the electrical conductivity of $La_{0.9}Me_{0.1}InO_{3-\delta}$. The composition $La_{0.9}Sr_{0.1}InO_{2.95}$ is characterized by the highest conductivity value, $7.6 \cdot 10^{-2}\ \Omega^{-1}\cdot cm^{-1}$ at 900 °C, in comparison with other alkaline earth metals. This result is probably due to the favorable combination of free migration volume and lattice expansion, with cation replacement occurring without much distortion, in comparison to other dopants.

The influence of the dopant concentration of calcium [43] and barium [66] substituted solid solutions is illustrated in Figure S3 and Figure S4, respectively. No previous reports have described similar data for strontium-containing solid solution. The data presented in literature focused on the electrical properties of the mono-doped $La_{0.9}Sr_{0.1}InO_{2.95}$ sample. In all substituted indates, an increase in conductivity in comparison with $LaInO_3$ is observed, resulting from the formation of oxygen vacancies as postulated by Equation 2.

The highest conductivity among calcium-containing phases (Figure S3) is observed for the sample LCI-10 from the homogeneous region. The activation energy of the substituted samples is within the range of 0.69–0.86 eV, which indicates that the predominant contribution to the conductivity in these samples is due to oxygen-ion transport.

The homogeneity region is markedly narrow ($x \leq 0.05$) when barium doping was used [66]. The $La_{0.95}Ba_{0.05}InO_{3-\delta}$ (LBI-5) sample exhibited the conductivity of $3 \cdot 10^{-5}\ \Omega^{-1}\times cm^{-1}$ at 500 °C (Figure S4). Nevertheless, a slight increase in conductivity is observed for the samples with higher concentration of barium. It can be reasonably assumed that the formation of a more symmetrical cubic structure in phases with $x > 0.1$ will result in an increase in electrical conductivity. Conversely, the decrease in electrical conductivity of the (LBI-15) sample may be correlated with the critical radius parameter of the oxygen migration channel r_{cr} [98]. In the perovskite structure, the migration of oxide ions is enabled by the oxygen pathway. The oxygen pathway is constrained by two A-site ions and one B-site ion, the radius of the inscribed circle of the oxygen pathway is referred to as the critical radius (see Figure 6).

The larger ionic radius of barium compared to that of lanthanum [27] leads to a narrowing of the critical radius of the O^{2-}-migration path, thereby explaining the decrease in ionic conductivity with increasing dopant concentration. Therefore, the increase in oxygen vacancies is compensated for by the decrease in effective pathways and ion transport. Consequently, the ionic conductivity of Ba-substituted $LaInO_3$ is strongly dependent on the distribution of the dopant [54, 71].

The transport properties of cubic lanthanum indates were subjected to the comprehensive study in the literature [70–74]. In the $La_{1-x}Ba_xInO_{3-\delta}$ ($0.4 \leq x \leq 0.8$) system, the $La_{0.6}Ba_{0.4}InO_{2.8}$ sample exhibits the highest conductivity of $3.16 \cdot 10^{-2}\ \Omega^{-1}\times cm^{-1}$ at 350 °C (Figure S5), a value that is higher than those observed for compounds with greater oxygen deficiency. The observed decrease in conductivity with increasing barium concentration can be attributed to two main factors. First, the symmetry is reduced from cubic to tetragonal crystal system. Second, there is an association between dopant cations and oxygen vacancies. The experimental data were confirmed using classical molecular dynamics methods [73].

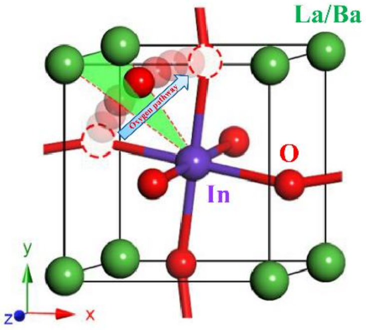

Figure 6 Illustration of the two-dimensional curved pathway for oxygen migration. Reproduced from ref. [99]. Copyright 2018, American Chemical Society.

The substitutions in the B-sublattice were described in only a small number of studies [44, 45, 80]. In work [44], the composition $LaIn_{0.9}Zr_{0.1}O_{3+\delta}$ was obtained, exhibiting a conductivity even lower than that of the base composition (illustrated in Figure 7). Furthermore, the authors observed that at low partial oxygen pressures the material undergoes decomposition. The electrical characteristics were improved by the introduction of the Sn^{2+} ion with a concentration of 3 mol% [80]. The conductivity of the Zn-doped (5–7 mol%) samples [45] was approximately two orders of magnitude higher than that of the parent system.

4.3. Electrical properties of co-doped $LaInO_3$ materials

The substitution of lanthanum with strontium significantly enhances the electrical conductivity of lanthanum indate, thereby stimulating further interest in identifying an appropriate B-sublattice co-dopant. The influence of double replacement by alkaline earth metals [52, 82], specifically $Sr^{2+} \rightarrow La^{3+}$ and $Ca^{2+}/Mg^{2+} \rightarrow In^{3+}$, acting as acceptor dopants within the *A*- and *B*-sublattices, respectively, was considerable (~3 orders of magnitude). This effect is achieved by the formation of twice as many oxygen vacancies. In the case of joint acceptor and donor substitution of Sr^{2+}/Zr^{4+} [44] with the same concentration of dopants, the oxygen vacancy concentration is smaller in comparison to that observed in double acceptor doping. Consequently, the conductivity of these materials may be slightly lower than that of acceptor-co-doped materials. The conductivity of the co-doped samples is presented in Figure 7, where a comparison with the mono-doped materials is also shown.

Figure 7 demonstrates that acceptor doping effectively improves electrical properties. All the presented solid solutions exhibited enhanced electrical conductivity in comparison to the matrix compound $LaInO_3$. Among all investigated phases with substituted A-cation, strontium- (10 mol%) [31] and barium-containing (40 mol%) phases exhibited the highest conductivity. Among the B-doped phases, zinc-containing compounds exhibited the greatest increase in electrical conductivity [45]. The highest level of conductivity among co-doped phases is observed for the compositions $La_{0.4}Pr_{0.4}Sr_{0.2}In_{0.8}Mg_{0.2}O_{3-\delta}$ [83] and $La_{0.9}Sr_{0.1}In_{0.9}Ca_{0.1}O_{3-\delta}$ [52]. The introduction of zirconium into the B-sublattice, specifically via the donor doping method, proved to be an ineffective strategy. The resulting conductivity of the sample was even lower than that of the parent compound.

An increase in ionic conductivity depends on two factors: the concentration of defects and their mobility. As anticipated, the conductivity increased with increasing dopant concentration. This was demonstrated for the calcium-doped $La_{0.95}Ca_{0.05}InO_{3-\delta}$ and $La_{0.9}Ca_{0.1}InO_{3-\delta}$ samples (Figure S3). A comparable behavior is observed in co-doped phases, wherein the total concentration of dopants reaches 20–30 mol% in $La_{0.9}Sr_{0.1}In_{0.9}Ca_{0.1}O_{3-\delta}$ (LSIC) [52] and $La_{0.8}Sr_{0.2}In_{0.9}Zr_{0.1}O_{3+\delta}$ (LSIZr20) [44].

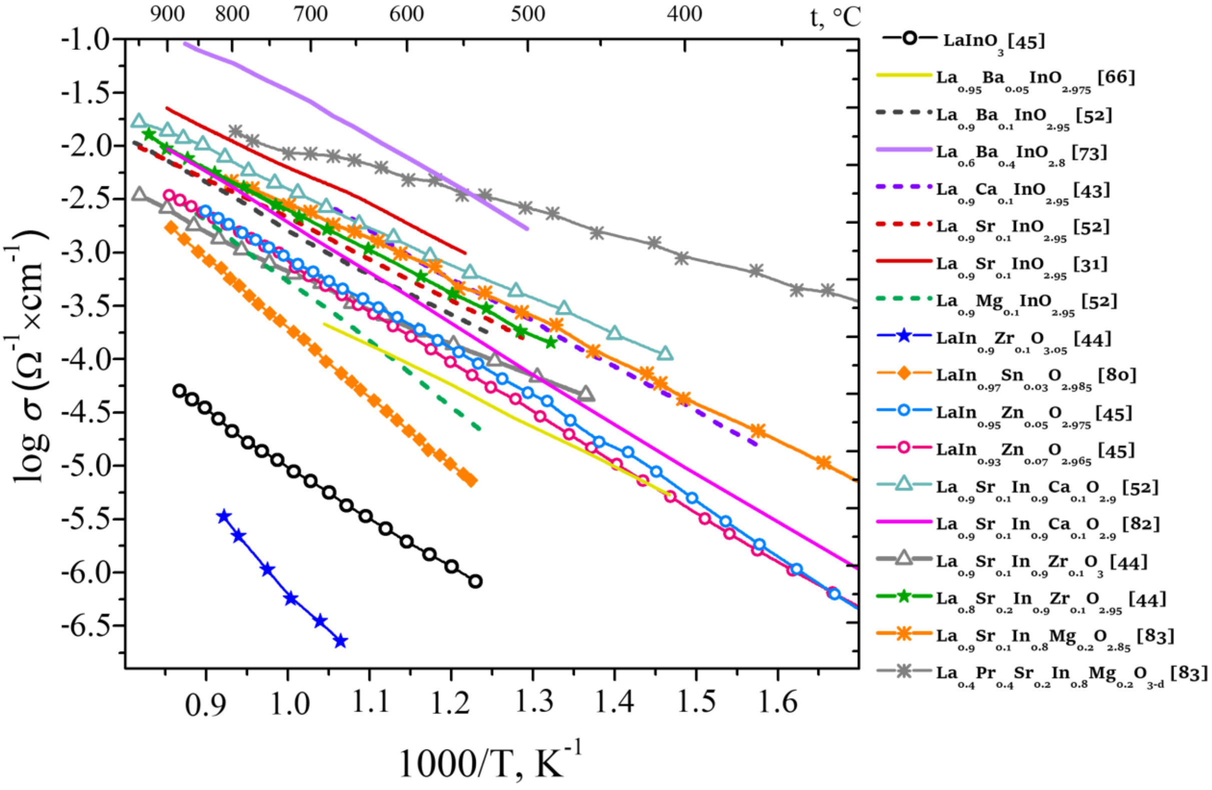

Figure 7 Temperature dependencies pure [45] and doped $LaInO_3$ materials: $La_{0.9}Ca_{0.1}InO_{3-\delta}$ (LCI10) [43]; $La_{0.9}Mg_{0.1}InO_{3-\delta}$ (LMI10) [52]; $La_{0.9}Sr_{0.1}InO_{3-\delta}$ (LSI10) [31, 52]; $La_{0.95}Ba_{0.05}InO_{3-\delta}$ (LBI05) [66]; $La_{0.9}Ba_{0.1}InO_{3-\delta}$ (LBI10) [52]; $La_{0.6}Ba_{0.4}InO_{3-\delta}$ (LBI40) [73]; $LaIn_{0.97}Sn_{0.03}O_{3-\delta}$ (LISn03) [80]; $LaIn_{0.9}Zr_{0.1}O_{3+\delta}$ (LIZr10) [44]; $LaIn_{0.95}Zn_{0.05}O_{2.975}$ (LIZ05) [45]; $LaIn_{0.95}Zn_{0.05}O_{2.975}$ (LIZ07) [45]; $La_{0.8}Sr_{0.2}In_{0.9}Zr_{0.1}O_{3+\delta}$ (LSIZr20) [44]; $La_{0.9}Sr_{0.1}In_{0.9}Zr_{0.1}O_{3+\delta}$ (LSIZr10) [44], $La_{0.9}Sr_{0.1}In_{0.9}Ca_{0.1}O_{3-\delta}$ (LSIC) [52,82], $La_{0.9}Sr_{0.1}In_{0.8}Mg_{0.2}O_{3-\delta}$ (LSIM) [83] and $La_{0.4}Pr_{0.4}Sr_{0.2}In_{0.8}Mg_{0.2}O_{3-\delta}$ [83].

The most significant effect of increase of conductivity is evident in the $La_{0.95}Ba_{0.05}InO_{3-δ}$ (LBI05) [66] and $La_{0.6}Ba_{0.4}InO_{3-δ}$ (LBI40) [73] phases (Figure 7). Moreover, the observed increase in conductivity can be attributed to the formation of a high-symmetry cubic structure.

The mobility of the defect may be dependent upon the geometric parameters of the structure. To illustrate a generally accepted approach, the "*free volume cell*" value (V_{free}) can be employed as a geometric parameter. The relationship between the electrical conductivities and the calculated values of cell volume and free cell volume for solid solutions based on $LaInO_3$ are presented in Table S2. Figure 8 shows the electrical conductivities at 650 °C for solid solutions based on $LaInO_3$ as a function of the free volume of the cell V_{free}. The ionic radius for XII-fold coordination in the case of $La_{0.9}Mg_{0.1}InO_{3-δ}$ was obtained using an approximation to the dependence of (r_{XII}/r_{VI}) versus (r_{VIII}/r_{VI}) for Me^{2+}-cations, as shown on the Figure S6.

In the case of phases doped on the A-*sublattice* with the composition $La_{0.9}Me_{0.1}InO_{3-δ}$ (Me = Ba^{2+}, Sr^{2+}, Ca^{2+}, Mg^{2+}), the general trend of conductivity behavior remains the same for both volume and free volume of the cell. The sample with the composition $La_{0.9}Mg_{0.1}InO_{3-δ}$ exhibited the lowest level of conductivity, which can be attributed to the fact that this phase is characterized by the smallest lattice volume [52].

The introduction of zinc into the indium sublattice was shown to result in a relatively high level of conductivity among B-sublattice dopants, in comparison to other substituents. This is confirmed by the calculated values of V_{free}.

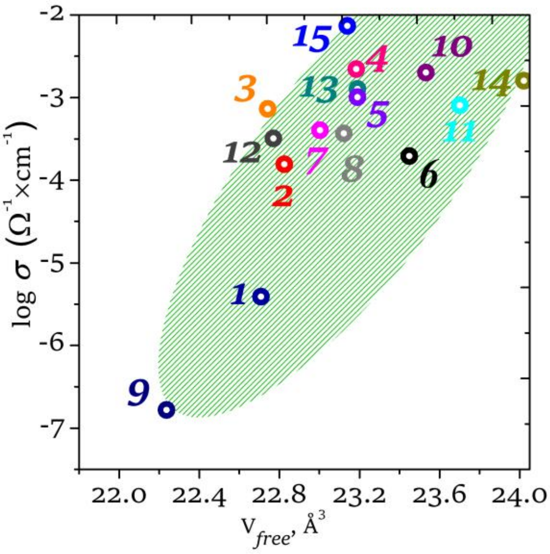

Figure 8 Conductivity values for initial (*1*) $LaInO_3$ and solid solutions: (*2*) – $La_{0.95}Ba_{0.05}InO_{3-δ}$ [66]; (*3*) –$La_{0.9}Ba_{0.1}InO_{3-δ}$ [52]; (*4*) –$La_{0.9}Ca_{0.1}InO_{3-δ}$ [43]; (*5*) – $La_{0.9}Sr_{0.1}InO_{3-δ}$ [52]; (*6*) –$La_{0.9}Mg_{0.1}InO_{3-δ}$ [52]; (*7*) –$LaIn_{0.95}Zn_{0.05}O_{2.975}$ [45], (*8*) – $LaIn_{0.93}Zn_{0.07}O_{2.965}$ [45], (*9*) – $LaIn_{0.9}Zr_{0.1}O_{3+δ}$ [44]; (*10*) – $La_{0.9}Sr_{0.1}In_{0.9}Ca_{0.1}O_{3-δ}$ [52], (*11*) – $La_{0.9}Sr_{0.1}In_{0.9}Ca_{0.1}O_{3-δ}$ [82]; (*12*) – $La_{0.9}Sr_{0.1}In_{0.9}Zr_{0.1}O_3$ [44]; (*13*) – $La_{0.8}Sr_{0.2}In_{0.9}Zr_{0.1}O_{3-δ}$ [44], (*14*) – $La_{0.9}Sr_{0.1}In_{0.8}Mg_{0.2}O_{3-δ}$ [83] and (*15*) –$La_{0.4}Pr_{0.4}Sr_{0.2}In_{0.8}Mg_{0.2}O_{2.8}$ [83].

These results demonstrate the success of acceptor doping as a method for producing oxygen-deficient and highly conductive compounds based on $LaInO_3$. A general trend of increasing electrical conductivity with increasing free cell volume V_{free} of lanthanum indate-based samples was identified.

4.4. The nature of conductivity of doped $LaInO_3$ materials

The solid solutions based on $LaInO_3$, as the parent compound, exhibit a mixed conductivity that is ionic and hole contributions. This behavior was observed for both mono-doped [31, 45] and co-doped materials (Figures S7–S8) [82].

However, as the temperature decreases, ionic transport becomes the dominant mechanism in most known lanthanum indate-doped materials. It is notable that in the study [68] *n*-type conductivity was also observed at low partial pressure of oxygen values.

4.5. Proton transport in doped $LaInO_3$

This section presents a summary of the experimental data on proton conductivity in substituted $LaInO_3$. As shown in Table S1, the doped phases are characterized by an effective anion radius exceeding 1.4; this criterion allows assuming the possibility of absorbing water from the gas phase and exhibiting proton conductivity (unlike aluminates and gallates). The total conductivity as a function of oxygen partial pressure in dry air and in 4.2% H_2O atmosphere presented in Figure S8 for the examples $La_{0.9}Sr_{0.1}InO_{2.95}$ [31] and $LaIn_{0.93}Zn_{0.07}O_{2.97}$ [45]. At elevated temperatures (700–800 °C), the samples exhibited a mixed type of conductivity in both dry and humid atmospheres [31, 45]. However, as the temperature decreases, a tendency towards a decrease in the positive slope of total conductivity at high pO_2 is observed, indicating an increase in the ionic contribution to the conductivity.

A comparison of the total electrical conductivity in dry and humid atmospheres reveals that in air (at $pO_2 = 0.21$ atm) the samples exhibit a relatively weak response to changes in humidity [31, 45]. The presence of hole defects and subsequent decrease in their concentration during proton incorporation does not make it possible to observe the effect of increasing the total conductivity in a humid atmosphere. However, this effect is observed in the intermediate and low pO_2 region (areas of low hole concentrations). The decrease in the concentration of more mobile hole carriers compared to proton defects occurs in accordance with the equation:

$$H_2O + 2h^{\bullet} + 2O_O^{x} \leftrightarrow {}^{1}\!/_{2}\,O_2 + 2(OH)_O^{\bullet}. \qquad (5)$$

The proton conductivity of doped $LaInO_3$ was investigated in several works [29–31, 45, 74, 84, 85]. Figure 9 presents the data on proton conductivity for mono-doped phases, namely $La_{0.9}Sr_{0.1}InO_{2.95}$ [29, 31, 85], $La_{0.6}Ba_{0.4}InO_{3-δ}$ [74], $LaIn_{0.93}Zn_{0.07}O_{2.975}$ [45] and $LaIn_{0.5}Zn_{0.5}O_{2.75}$.

Furthermore, the data include co-doped samples $La_{0.9}Sr_{0.1}In_{0.9}Mg_{0.1}O_{3-\delta}$ [30], $La_{0.6}Ba_{0.4}In_{0.75}Yb_{0.25}O_{3-\delta}$ [74] and $La_{0.5}Ba_{0.5}In_{0.5}Yb_{0.5}O_{3-\delta}$ [84] samples. The activation energy of proton conductivity was estimated within the temperature range of 300–600 °C, and the resulting values are presented in Table S3. A comparison of relative densities is also presented in Table S3. As can be seen, the investigations were performed under different conditions, thus the comparative analysis demonstrates the general trends.

The $La_{0.9}Sr_{0.1}InO_{2.95}$ sample exhibits one of the highest proton conductivity values. Moreover, the proton conductivities of LSI10 (lines ***1***, ***2*** and ***3***) described in the works [29, 31, 85] are in agreement with one another. These phases exhibit the typical E_a (~0.5 eV) values associated with the Grotthuss mechanism of proton transport [101, 102]. The incorporation of strontium as a dopant into the lanthanum positions is complete due to the lowest dissolution energy (Figure 2). As a result, La^{3+} (r = 1.36 Å for the XII-fold coordination [27]) and Sr^{2+} (1.44 Å, for the XII-fold coordination) are the most suitable A-site ions for improving conductivity [103]. The observation that the Sr^{2+}-doped samples exhibit the highest proton conductivity among alkaline earth dopants is a common property for many $LaB^{3+}O_3$ systems.

The introduction of Ba^{2+} into La-sites was performed at a high concentration of the dopant, leading to the creation of a high concentration of oxygen vacancies capable of incorporation of water. Moreover, $La_{0.6}Ba_{0.4}InO_{3-\delta}$ sample is characterized by high-symmetry cubic structure. Therefore, it can be expected that these factors will result in an even higher level of proton conductivity. However, the Ba^{2+}-doped sample (line ***4*** on Figure 9) exhibits a lower proton conductivity than the strontium-doped sample, and its E_a value is the highest among the samples. As shown in Table S3, the conductivity was measured in a humid nitrogen atmosphere.

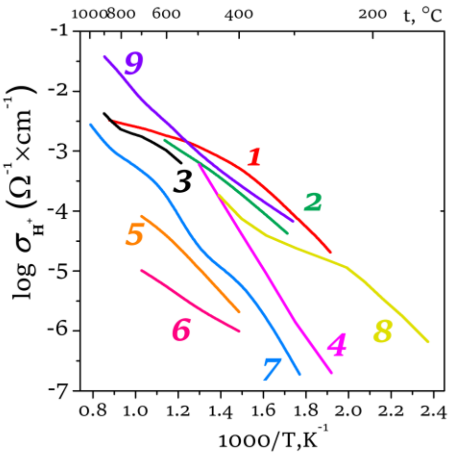

Figure 9 The proton conductivity for $La_{0.9}Sr_{0.1}InO_{2.95}$ (LSI10): **1** – [29], **2** –[85], **3** –[31]; **4** – $La_{0.6}Ba_{0.4}InO_{3-\delta}$ (LBI40) [74]; **5** – $LaIn_{0.93}Zn_{0.07}O_{2.975}$ (LIZ07) [45]; **6** – $LaIn_{0.5}Zn_{0.5}O_{2.75}$ (LIZ50) [100]; **7** – $La_{0.9}Sr_{0.1}In_{0.9}Mg_{0.1}O_{3-\delta}$ (LSIM10) [30], **8** – $La_{0.6}Ba_{0.4}In_{0.75}Yb_{0.25}O_{3-\delta}$ (LBIY40) [74], and **9** – $La_{0.5}Ba_{0.5}In_{0.5}Yb_{0.5}O_{3-\delta}$ (LBIY50) [84] samples.

In contrast, the conductivity of other samples was measured in a hydrogen-containing atmosphere. As a result, the proton transport level cannot be compared.

Additionally, the incorporation of a substantial quantity of negative charged acceptor defects may lead to defect association and consequently decrease the concentration of available oxygen vacancies, thereby reducing the proton conductivity [87, 88] A similar effect is observed in the case of samples containing zinc (line ***5***, ***6***).

The co-doping Sr^{2+}/Mg^{2+} (line ***7*** on the Figure 9) resulted in a decrease in proton transport, initially induced by Sr^{2+}-doping. These results are difficult to interpret due to the absence of comprehensive data related to the experiment description. Additionally, the authors [30] have claimed that the LSIM sample exhibited degradation during the measurements.

The co-doped samples $Ba^{2+} \rightarrow La^{3+}$ /$Yb^{3+} \rightarrow In^{3+}$ (line ***8*** and ***9*** on Figure 9) exhibit high proton conductivity. The Yb^{3+} is an isovalent dopant that does not affect the concentration of oxygen vacancies. However, the ionic radius of the Yb^{3+} cation (r = 0.868 Å for the VI-fold coordination) is larger than that of the In^{3+} cation (r = 0.800 Å for the VI-fold coordination) [27], resulting in an expansion of the unit cell, which is a favorable factor for enhanced proton transport.

As shown in Figures 7–9, the use of various acceptor dopants, especially alkaline earth elements, led to a noticeable increase in the conductivity of $LaInO_3$. However, the presence of alkaline earth elements is undesirable from the point of view of possible deterioration of chemical stability, as was observed for $A^{2+}B^{4+}O_3$ perovskites. A detailed discussion of the chemical stability of doped $LaInO_3$ is presented in Section 5. Nevertheless, the $LaInO_3$ system is doped at relatively low concentrations, which will have a minor impact on chemical stability compared to the benefit of a significant impact on electrical conductivity levels.

The proton conductivity of substituted lanthanum indate was compared with that of other $LaBO_3$ perovskites. The most commonly discussed solid solutions containing Sr^{2+} in the La-sites were selected for comparison. Figure 10 shows the temperature dependence of the proton conductivity of $La_{0.9}Sr_{0.1}B^{3+}O_{3-\delta}$ (B^{3+} = Sc, In, Yb, Y) materials. Table S4 compares proton conductivity activation energies, relative densities, and measurement conditions for $La_{0.9}Sr_{0.1}B^{3+}O_{3-\delta}$ phases. Furthermore, the data for known proton conductors, doped $BaCe(Zr)O_3$, are provided in Figure 10 for additional comparison.

As seen in Figure 10, the proton conductivity of known proton conductors based on $BaCe(Zr)O_3$ is higher than that of $LaB^{3+}O_3$. Nevertheless, the proton conductivity of $La_{0.9}Sr_{0.1}InO_{3-\delta}$ samples is comparable to that for $BaZr_{0.8}Y_{0.2}O_{3-\delta}$ materials (line 7) and even exceeds it (line 6) at T < 400 °C. Thus, Sr-substituted $LaInO_3$ phase have acceptable level of proton conductivity.

DOI: 10.15826/chimtech.2025.12.1.11

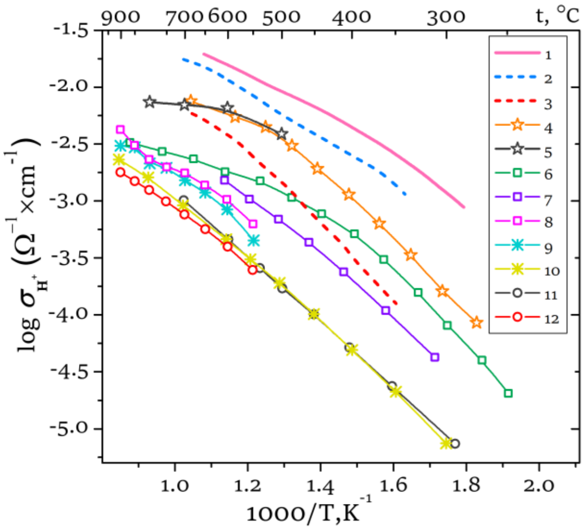

Figure 10 The proton conductivity for (***1***) – $BaCe_{0.7}Zr_{0.1}Y_{0.2}O_{3-\delta}$ [104]; (***2***) – $BaCe_{0.8}Y_{0.2}O_{3-\delta}$ [104]; (***3***) – $BaZr_{0.8}Y_{0.2}O_{3-\delta}$ [104]; $La_{0.9}Sr_{0.1}ScO_{2.95}$: (***4***) – [105], (***5***) – [29]; $La_{0.9}Sr_{0.1}InO_{2.95}$: (***6***) –[29], (***7***) – [85], (***8***) – [31]; $La_{0.9}Sr_{0.1}YbO_{2.95}$: (***9***) – [37], (***10***) – [106]; and $La_{0.9}Sr_{0.1}YO_{2.95}$ (***11***) – [29], (***12***) – [31] samples.

The protonic transport of $La_{0.9}Sr_{0.1}B^{3+}O_{3-\delta}$ samples increased in the following series of substituents: Y = Yb<In<Sc. The relationships between the proton transport of lanthanum-containing perovskites and their composition were discussed in the works [28–30].

Figure 11 shows the protonic transport numbers of the $La_{0.9}Sr_{0.1}B^{3+}O_{3-\delta}$ (B^{3+} = Al, Ga, Sc, In, Yb, Y) samples [29] and their correlation with anion radii values. The radii anion values were calculated from the available unit cell parameters outlined [31, 35, 37, 82, 92, 105] and are presented in Table 2.

It can be discerned that a set of lanthanum-containing perovskites $LaB^{3+}O_3$ (where B^{3+} = Al, Ga, Sc, In, Yb, Y), exhibit a tendency towards certain regularities. The proton transport is absent from the phases characterized by a smaller anion radius, r_{an}, including those observed in aluminates and gallates, where the size of the B-cation is relatively small. Materials based on $LaYO_3$ and $LaYbO_3$ exhibit a predominantly proton transport nature and are characterized by increased r_{an} values and a large ionic radius of cations (Yb, Y). The remaining phases are typified by co-ionic transport, in which the role of proton transport becomes increasingly significant as the ionic radius of both the B cation and r_{an} increases.

Table 2 Structural characteristics and protonic transport numbers [29] for the $La_{0.9}Sr_{0.1}B^{3+}O_3$, ($B^{3+}$ = Al, Ga, Sc, In, Yb, Y) materials.

B^{3+}	rB^{3+} (Å)	$\tilde{V}_{cell}$ (Å³)	$\tilde{a}$ (Å)ᵃ	r_{an} (Å)	Σt_{H+}	[Ref.]
Al	0.535	54.39(1)	3.788(9)	1.383(3)	0.01	[31]
Ga	0.620	58.93(2)	3.891(5)	1.395(7)	0.01	[92]
Sc	0.745	66.98(2)	4.061(2)	1.425(3)	0.88	[105]
In	0.800	70.04(3)	4.122(1)	1.430(1)	0.67	[82]
Yb	0.868	73.99(5)	4.198(2)	1.436(4)	0.99	[37]
Y	0.900	75.52(5)	4.226(9)	1.435(2)	0.99	[35]

[a] Equivalent cubic unit cell parameter was calculated as the cube root of the $\tilde{V}_{cell}$.

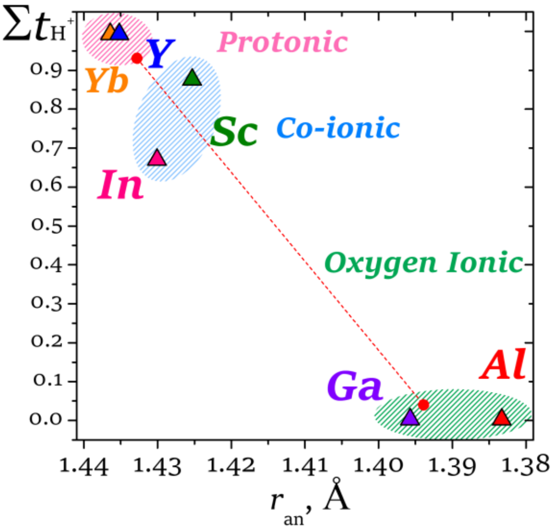

Figure 11 The protonic transport numbers [29] as a function of the r_{an} values for various $La_{0.9}Sr_{0.1}B^{3+}O_3$, ($B^{3+}$ = Al, Ga, Sc, In, Yb, Y), calculated with using XRD data from the works [31, 35, 37, 82, 92, 105].

5. Chemical stability in CO_2 and H_2

The pure $LaInO_3$ complex oxide, as well as other lanthanum-containing perovskites, is chemically stable towards to components of the gas atmosphere. The introduction of an alkaline earth element as a dopant, even at comparatively low concentrations, can result in the degradation of the $LaInO_3$ materials. He et al. [31] investigated a chemical stability $La_{0.9}Sr_{0.1}InO_{2.95}$ sample in reducting atmosphere. The peaks of indium metal in the XRD pattern were observed after exposure to 1% H_2 atmosphere. When the concentration of H_2 reached 20% H_2, an additional phase of La_2SrO_x was formed. In addition, the sample demonstrated poor chemical stability in a carbon oxide atmosphere comprising 80% CO / 20% CO_2. That is, at certain concentrations of alkaline earth metal dopants, the oxides lose chemical stability [52].

In contrast to alkaline earth elements, a the presence of zinc as a dopant does not lead to a deterioration in chemical resistance [45]. The chemical stability of Zn-doped samples treated in a carbon dioxide (50% CO_2 /50% air) atmosphere at temperatures up to 500 °C was confirmed by varying pO_2 and pH_2O conditions.

Therefore, it is important to determine the optimal composition of the material in order to achieve the desired chemical resistance and ensure its suitability for practical applications; for example, an acceptable strategy is to use two dopants with minimal concentrations: $Sr^{2+} \rightarrow La^{3+}$ and $Zn^{2+} \rightarrow In^{3+}$. Doping with strontium increases the conductivity of the material, while the introduction of zinc preserves its chemical composition and structure.

6. Thermomechanical properties

The $LaInO_3$-based materials have the potential to work effectively as electrolytes in SOFCs. For optimal and longterm functionality of electrochemical devices, it is critical to achieve appropriate thermomechanical compatibility between the electrolyte and electrode materials.

Table 3 lists the TEC values for $LaInO_3$-doped materials [43, 66, 69, 113, 114] in comparison with other electrolytes, including $LaB^{3+}O_3$ [33, 36, 37, 41, 115–117], $BaCeO_3$ [33], $BaZrO_3$ [104] and 8YSZ [118]. As seen, $LaInO_3$ materials are distinguished by their low values of thermal expansion coefficients (TEC, α), which is in the range between 6 and $10 \cdot 10^{-6}$ K^{-1}. In general, these values are similar to those of both the other lanthanum-containing perovskites and the well-known oxygen-ion electrolytes. These TEC values are in the range required for SOFC applications.

7. Limitations

One of the limitations of this study is the unavailability of data on the relative density for doped samples in the literature, which would facilitate a more detailed analysis of conductivity. Furthermore, there is a scarcity of data in the existing literature on the limits of hydration in doped samples and their proton conductivity. A comprehensive analysis of studies on proton transport, including proton conductivity and proton mobility, is possible since the investigations were carried out under different conditions.

Table 3 Average thermal expansion coefficients values for $LaInO_3$-materials and a set of known electrolytes.

Composition	Temperature range (K)	$\alpha \cdot 10^6$ (K^{-1})	[Ref.]
$LaInO_3$	200–873	6–9	[114]
$LaInO_3$	773–1273	8.79	[43]
$LaInO_3$	673–1073	8.72	[66]
$La_{0.95}Dy_{0.05}InO_3$	400–1000	7.37	[113]
$La_{0.95}Ho_{0.05}InO_3$	400–1000	7.77	[113]
$La_{0.95}Ho_{0.05}In_{0.98}Sb_{0.02}O_3$	400–1000	7.26	[113]
$La_{0.95}Ca_{0.05}InO_{2.975}$	773–1273	9.0	[43]
$La_{0.9}Ca_{0.1}InO_{2.95}$	773–1273	9.1	[43]
$La_{0.8}Sr_{0.2}InO_{2.9}$	773–1273	9.11	[69]
$La_{0.95}Ba_{0.05}InO_{2.975}$	673–1073	9.88	[66]
$LaAlO_3$	303–1200	11.4	[115]
$La_{0.8}Sr_{0.2}AlO_{3-\delta}$	303–1200	9.9	[115]
$La_{0.9}Sr_{0.1}Ga_{0.8}Mg_{0.2}O_{3-\delta}$	473–1473	11.4	[33]
$La_{0.95}Ba_{0.05}ScO_{3-\delta}$	298–1173	8.9	[41]
$La_{0.9}Sr_{0.1}ScO_{3-\delta}$	298–1173	8.5	[116]
$La_{0.9}Sr_{0.1}YO_{3-\delta}$	373–1273	10.7	[36]
$La_{0.9}Ca_{0.1}YbO_{3-\delta}$	373–1273	10.8	[37]
$La_{0.9}Sr_{0.1}YbO_{3-\delta}$	373–1273	11.7	[37]
$La_{0.8}Ca_{0.2}CrO_{3-\delta}$	298–1073	10.5	[117]
ZrO_2–(8 mol%)Y_2O_3	303–1273	10.9	[118]
$BaCe_{0.8}Y_{0.2}O_{3-\delta}$	893–1173	8.3	[33]
$BaZrO_3$	298–1675	7.5	[104]

8. Conclusions

The review summarizes the data on the structure, hydration processes, transport and thermomechanical properties, as well as the chemical stability of solid solutions based on $LaInO_3$. The use of a wide range of acceptor dopants, including alkaline earth elements, was demonstrated to enhance the transport properties. It was found that there is a general trend of increasing electrical conductivity with an increase in the value of the free cell volume. The highest conductivity is observed in mono- and co-doped materials containing strontium in the A-sublattice. Further prospects for the development of the materials based on $LaInO_3$ may be associated with the development of co-doped strategy, whereby the optimal balance between high conductivity and chemical stability can be achieved.

Supplementary information

This manuscript contains supplementary materials, which are available on the corresponding online page.

Data availability statement

Data sharing is not applicable to this article as no new data were created or analyzed in this study.

Acknowledgments

None.

Author contributions

Conceptualization: A.V.E., I.E.A.
Data curation: A.V.E., K.G.B.
Formal Analysis: A.V.E, K.G.B.
Funding acquisition: A.V.E.
Investigation: A.V.E., K.G.B.
Methodology: A.V.E., K.G.B.
Project administration: A.V.E.
Resources: A.V.E.
Supervision: A.V.E., I.E.A.
Visualization: A.V.E.
Writing – original draft: A.V.E., K.G.B., I.E.A.
Writing – review & editing: A.V.E., I.E.A.

Conflict of interest

The authors declare no conflict of interest.

Additional information

Author IDs:

Anastasia V. Egorova, Scopus ID 58040927300;
Ksenia G. Belova, Scopus ID 56509536000;
Irina I. Animitsa, Scopus ID 6603520951.

Websites:

Ural Federal University named after the first President of Russia B.N.Yeltsin, https://urfu.ru/ru/;

Institute of Solid State Chemistry, Ural Branch of the Russian Academy of Sciences, https://www.ihim.uran.ru/.

Brief biography

Anastasia V. Egorova, PhD, Senior Researcher in the Laboratory of Selectively Permeable Ceramics and Engineering, ISSC of RAS(UB). With over 8 years of relevant expertise, Anastasia is engaged in the development of proton oxide materials based on lanthanum indate and lanthanum aluminate with a perovskite structure for alternative energy devices.
ResearchGate page: Anastasia Egorova

Ksenia G. Belova, PhD, works as associate professor of the Department of Physical and Inorganic Chemistry at Ural federal university. Her research interests include the study of the physicochemical characteristics of perovskite materials with proton conductivity, with a view to determining their potential use as components in electrochemical devices. Ksenia is an expert in the field of thermal analysis, which enables her to conduct a extensive investigation into proton transport.
ResearchGate page: Ksenia Belova

Irina E. Animitsa, Doctor of Science, professor in the Department of Physical and Inorganic Chemistry at Ural federal university. Her proficiency in solid-state chemistry facilitated a critical assessment of the outcomes yielded. The methods of synthesis, defects, hydration processes, transport properties and the prospects of the complex oxides for various electrochemical applications were exhaustively studied under the supervision of I.E. Animitsa.
ResearchGate page: Irina Animitsa

References

1. Sikstrom D, Thangadurai V. A tutorial review on solid oxide fuel cells: fundamentals, materials, and applications. Ionics (Kiel). 2024. doi:10.1007/s11581-024-05824-7
2. Chun O, et al. Advances in low-temperature solid oxide fuel cells: An explanatory review. J Power Sources. 2024;610:234719. doi:10.1016/j.jpowsour.2024.234719
3. Singh M, Zappa D, Comini E. Solid oxide fuel cell: Decade of progress, future perspectives and challenges. Int J Hydrogen Energy. 2021;46:27643–74. doi:10.1016/j.ijhydene.2021.06.020
4. Qasem NAA, Abdulrahman GAQ. A Recent Comprehensive Review of Fuel Cells: History, Types, and Applications. Int J Energy Res. 2024;2024. doi:10.1155/2024/7271748
5. Coduri M, et al. Structure-property correlation in oxide-ion and proton conductors for clean energy applications: Recent experimental and computational advancements. J Mater Chem A. 2022;10:5052–110. doi:10.1039/d1ta10326a
6. Malik V, et al. Comparative study and analysis between Solid Oxide Fuel Cells (SOFC) and Proton Exchange Membrane (PEM) fuel cell - A review. Mater Today Proc. 2021;47:2270–5. doi:10.1016/j.matpr.2021.04.203
7. Tariq U, et al. Bridging the Gap between fundamentals and efficient devices: Advances in proton-conducting oxides for low-temperature solid oxide fuel cells. J Power Sources. 2024;613:234910. doi:10.1016/j.jpowsour.2024.234910
8. Irvine J, et al. Roadmap on inorganic perovskites for energy applications. JPhys Energy. 2021;3. doi:10.1088/2515-7655/abff18
9. Hanif MB, et al. Mo-doped $BaCe_{0.9}Y_{0.1}O_{3-\delta}$ proton-conducting electrolyte at intermediate temperature SOFCs. Part I: Microstructure and electrochemical properties. Int J Hydrogen Energy. 2023;48:37532–49. doi:10.1016/j.ijhydene.2023.01.144
10. Iwahara H, et al. Proton conduction in sintered oxides and its application to steam electrolysis for hydrogen production. Solid State Ionics. 1981;3–4:359–63. doi:10.1016/0167-2738(81)90113-2
11. Kreuer K-D. Proton Conductivity: Materials and Applications. Chem Mater. 1996;8:610–41. doi:10.1021/cm950192a
12. Chen G, et al. Ionic conduction mechanism of a nanostructured BCY electrolyte for low-temperature SOFC. Int J Hydrogen Energy. 2020;45:24108–15. doi:10.1016/j.ijhydene.2019.07.223
13. Matsuda RM, et al. Sintering mechanism and electrical conductivity of ZnO added $BaCe_{0.8}Zr_{0.1}Y_{0.1}O_{3-\delta}$ proton conducting perovskites. Solid State Ionics. 2023;403:116407. doi:10.1016/j.ssi.2023.116407
14. Soares HS, et al. Effect of the addition mechanism of ZnO sintering aid on densification, microstructure and electrical properties of $Ba(Zr,Y)O_{3-\delta}$ proton-conducting perovskite. Int J Hydrogen Energy. 2021;46:26466–77. doi:10.1016/j.ijhydene.2021.05.109
15. Ebert JN, et al. Bulk and grain boundary conductivity in doped $BaZrO_3$: Bulk contribution dominates at operating temperatures. Scr Mater. 2024;241:0–5. doi:10.1016/j.scriptamat.2023.115852
16. Kindelmann M, et al. Controlling grain boundary segregation to tune the conductivity of ceramic proton conductors. ChemRxiv. 2024. doi:10.26434/chemrxiv-2024-svz4w
17. Duan C, et al. Proton-conducting oxides for energy conversion and storage. Appl Phys Rev. 2020;7. doi:10.1063/1.5135319
18. Sažinas R, Bernuy-López C, Einarsrud MA, Grande T. Effect of CO2 Exposure on the Chemical Stability and Mechanical Properties of $BaZrO_3$-Ceramics. J Am Ceram Soc. 2016;99:3685–95. doi:10.1111/jace.14395
19. Somekawa T, et al. Physicochemical properties of $Ba(Zr,Ce)O_{3-\Delta}$-based proton-conducting electrolytes for solid oxide fuel cells in terms of chemical stability and electrochemical performance. Int J Hydrogen Energy. 2017;42:16722–30. doi:10.1016/j.ijhydene.2017.04.267
20. Luo Y, et al. Chemical stability and electrical properties of $Ba_{1-x}Ca_xCe_{0.8}Gd_{0.2}O_{3-\delta}$ ($0 \le x \le 0.06$) proton conductor. Int J Hydrogen Energy. 2023;48:5656–67. doi:10.1016/j.ijhydene.2022.11.072
21. Hashim SS, et al. Perovskite-based proton conducting membranes for hydrogen separation: A review. Int J Hydrogen Energy. 2018;43:15281–305. doi:10.1016/j.ijhydene.2018.06.045
22 Peng X, et al. A double perovskite decorated carbon-tolerant redox electrode for symmetrical SOFC. Int J Hydrogen Energy. 2020;45:14461–9. doi:10.1016/j.ijhydene.2020.03.151
23. Chen Y, et al. Advances in Cathode Materials for Solid Oxide Fuel Cells: Complex Oxides without Alkaline Earth Metal Elements. Adv Energy Mater. 2015;5:1–34. doi:10.1002/aenm.201500537
24. Tarutin AP, et al. Chemical design of oxygen electrodes for solid oxide electrochemical cells: A guide. Sustain Energy Technol Assessments. 2023;57:103185. doi:10.1016/j.seta.2023.103185.
25. Qiu P, et al. Materials of solid oxide electrolysis cells for H2 O and CO_2 electrolysis: A review. J Adv Ceram. 2023;12:1463–510. doi:10.26599/JAC.2023.9220767
26. Li C, Soh KCK, Wu P. Formability of ABO_3 perovskites. J Alloys Compd 2004;372:40–8. doi:10.1016/j.jallcom.2003.10.017
27. Shannon RD. Revised effective ionic radii and systematic studies of interatomic distances in halides and chalcogenides. Acta Crystallogr Sect A. 1976;32:751–67. doi:10.1107/S0567739476001551
28. Kasyanova AV, et al. Lanthanum-Containing Proton-

Conducting Electrolytes with Perovskite Structures. Membr Membr Technol. 2021;3:73–97. doi:10.1134/S2517751621020050

29. Okuyama Y, et al. Incorporation and conduction of proton in Sr-doped $LaMO_3$ (M=Al, Sc, In, Yb, Y). Electrochim Acta. 2014;125:443–9. doi:10.1016/j.electacta.2014.01.113
30. Lybye D, Poulsen FW, Mogensen M. Conductivity of A- and B-site doped $LaAlO_3$, $LaGaO_3$, $LaScO_3$ and $LaInO_3$ perovskites. Solid State Ionics. 2000;128:91–103. doi:10.1016/S0167-2738(99)00337-9
31. He C, Wu J, Lee Y. Correlation between conductivity and structural parameters in Sr-doped $LaMO_3$ (M = Al, Ga, In, Er, and Y) for solid oxide membranes. Solid State Ionics. 2023;399:116315. doi:10.1016/j.ssi.2023.116315
32. Yu J, et al. Ionic conductivity and crystal structure of LSGM with different element mole ratios. Fuel Cells. 2021;21:149–54. doi:10.1002/fuce.202000056
33. Gordeev E V, Porotnikova NM. Approaches for the preparation of dense ceramics and sintering aids for Sr/Mg doped lanthanum gallate: focus review. Electrochem Mater Technol. 2023;2:20232022. doi:10.15826/elmattech.2023.2.022
34. Villas-Boas LA, Goulart CA, De Souza DPF. Effects of Sr and Mn co-doping on microstructural evolution and electrical properties of $LaAlO_3$. Process Appl Ceram. 2019;13:333–41. doi:10.2298/PAC1904333V
35. Kalyakin A, et al. Characterization of proton-conducting electrolyte based on $La_{0.9}Sr_{0.1}YO_{3-\delta}$ and its application in a hydrogen amperometric sensor. Sensors Actuators B Chem. 2016;225:446–52. doi:10.1016/j.snb.2015.11.064
36. Kasyanova A, et al. Thermal and Electrical Properties of Highly Dense Ceramic Materials Based on Co-doped $LaYO_3$. Jom. 2019;71:3789–95. doi:10.1007/s11837-019-03498-5
37. Kasyanova AV, et al. Transport properties of $LaYbO_3$-based electrolytes doped with alkaline earth elements. Electrochim Acta. 2023;439:141702. doi:10.1016/j.electacta.2022.141702
38. Kasyanova AV., et al. Low-temperature transport properties of isovalent-substituted $La_{0.9}Sr_{0.1}YbO_{3-\delta}$ ceramic materials. J Solid State Electrochem. 2023. doi:10.1007/s10008-023-05574-y
39. Antonova EP. Proton-conducting oxides based on $LaScO_3$: structure, properties and electrochemical applications. A focus review. Electrochem Mater Technol. 2023;2:20232021. doi:10.15826/elmattech.2023.2.021
40. Belova KG, et al. Conductivity and chemical stability of co-doped $LaScO_3$ ceramics. Ceram Int. 2024;50:40321–9. doi:10.1016/j.ceramint.2024.06.148
41. Lesnichyova A, et al. Densification and Proton Conductivity of $La_{1-x}Ba_xScO_{3-\delta}$ Electrolyte Membranes. Membranes (Basel). 2022;12. doi:10.3390/membranes12111084
42. Belyakov SA, et al. Dopant-induced changes of local structures for adjusting the hydration ability of proton-conducting lanthanum scandates. J Mater Chem A. 2023;11:19605–18. doi:10.1039/D3TA03673A
43. Sood K, et al. Preferential occupancy of Ca^{2+} dopant in $La_{1-x}Ca_xInO_{3-\delta}$ (x = 0–0.20) perovskite: structural and electrical properties. Ionics (Kiel). 2015;21:2839–50. doi:10.1007/s11581-015-1461-8
44. He H, Huang X, Chen L. The effects of dopant valence on the structure and electrical conductivity of $LaInO_3$. Electrochim Acta. 2001;46:2871–7. doi:10.1016/S0013-4686(01)00508-4
45. Egorova A V., Belova KG, Animitsa IE. Ionic (O^{2-}, H^+) transport in novel Zn-doped perovskite $LaInO_3$. Int J Hydrogen Energy. 2023;48:22685–97. doi:10.1016/j.ijhydene.2023.03.263
46. Keith ML, Roy R. Structural relations among double oxides of trivalent elements. Am Mineral J Earth Planet Mater. 1954;39:1–23.
47. Roth RS. Classification of Perovskite and Other ABO_3-Type. J Res Natl Bur Stand. 1957;58:75. doi:10.6028/jres.058.010
48. Ruiz-Trejo E, Tavizón G, Arroyo-Landeros A. Structure, point defects and ion migration in $LaInO_3$. J Phys Chem Solids. 2003;64:515–21. doi:10.1016/S0022-3697(02)00358-X
49. Hartley P, et al. Experimental and Theoretical Study of the Electronic Structures of Lanthanide Indium Perovskites $LnInO_3$. J Phys Chem C. 2021;125:6387–400. doi:10.1021/acs.jpcc.0c11592
50. Park HM, et al. Lanthanum indium oxide from X-ray powder diffraction. Acta Crystallogr Sect C. 2003;59:i131–i132. doi:10.1107/S0108270103024806
51. Hu T, et al. Dy^{3+}-doped $LaInO_3$: a host-sensitized white luminescence phosphor with exciton-mediated energy transfer. J Mater Chem C. 2021;9:13410–9. doi:10.1039/d1tc01317c
52. He H, Huang X, Chen L. Sr-doped $LaInO_3$ and its possible application in a single layer SOFC. Solid State Ionics. 2000;130:183–93. doi:10.1016/S0167-2738(00)00666-4
53. Srivastava AM, et al. Spectroscopy of Mn^{4+} in orthorhombic perovskite, $LaInO_3$. J Lumin. 2019;206:398–402. doi:10.1016/j.jlumin.2018.10.090
54. Hwang KJ, et al. Molecular dynamics simulation of oxygen ion conduction in orthorhombic perovskite Ba-doped $LaInO_3$ using cubic and orthorhombic model. J Nanosci Nanotechnol. 2015;15:8947–50. doi:10.1166/jnn.2015.11540
55. Yukhno E, et al. Excitation and emission spectra of $LaInO_3$-based solid solutions doped with Sm^{3+}, Sb^{3+}. J Lumin. 2017;182:123–9. doi:10.1016/j.jlumin.2016.10.020
56. Kamal CS, et al. Unravelling the energy transfer mechanism in bismuth co-activation of $LaInO_3$:Sm^{3+}/Ho^{3+} nanophosphor for color-tunable luminescence. RSC Adv. 2017;7:9724–31. doi:10.1039/C6RA28719K
57. Yukhno EK, et al. Magnetic properties of $LaInO_3$-based perovskite-structure photoluminescent materials doped with Nd^{3+}, Cr^{3+}, and Mn^{3+} ions. Inorg Mater. 2016;52:218–24. doi:10.1134/S0020168516010155
58. Hu X, Piccinelli F, Bettinelli M. White light emission and energy transfer processes in $LaInO_3$ doped with Bi^{3+}, Tb^{3+} and Eu^{3+}. J Alloys Compd. 2022;899:163344. doi:10.1016/j.jallcom.2021.163344
59. Lakshminarasimhan N, Varadaraju UV. Luminescent host lattices, $LaInO_3$ and $LaGaO_3$—A reinvestigation of luminescence of d10 metal ions. Mater Res Bull. 2006;41:724–31. doi:10.1016/j.materresbull.2005.10.010
60. Dhanasekaran P, Gupta NM. Effects of grain morphology, microstructure and dispersed metal cocatalyst on the photoreduction of water over impurity-doped $LaInO_3$. Mater Res Bull. 2012;47:1217–28. doi:10.1016/j.materresbull.2012.01.031
61. Nomura K, Tanase S. Electrical conduction behavior in $(La_{0.9}Sr_{0.1})M^{III}O_{3-\delta}$ (M^{III} = Al, Ga, Sc, In, and Lu) perovskites. Solid State Ionics. 1997;98:229–36. doi:10.1016/s0167-2738(97)00101-x
62. Cook RL, Sammells AF. On the systematic selection of perovskite solid electrolytes for intermediate temperature fuel cells. Solid State Ionics. 1991;45:311–21. doi:10.1016/0167-2738(91)90167-A
63. Sammells AF, et al. Rational selection of advanced solid electrolytes for intermediate temperature fuel cells. Solid State Ionics. 1992;52:111–23. doi:10.1016/0167-2738(92)90097-9
64. Ranløv J, et al. Criteria for prediction of high oxide ion conductivity in perovskite oxides. Solid State Phenom. 1994;39:219–22.
65. Levy MR, Steel BCH, Grimes RW. Divalent cation solution in $A^{3+}B^{3+}O_3$ perovskites. Solid State Ionics. 2004;175:349–52. doi:10.1016/j.ssi.2004.02.072
66. Sood K, Singh K, Pandey OP. Co-existence of cubic and orthorhombic phases in Ba-doped $LaInO_3$ and their effect on conductivity. Phys B Condens Matter. 2015;456:250–7. doi:10.1016/j.physb.2014.08.036
67. Sood K, Singh K, Pandey OP. Study of the Structural and Electrical Behaviour of Ca Doped $LaInO_3$ Electrolyte Material. Trans Indian Ceram Soc. 2013;72:32–5. doi:10.1080/0371750X.2013.795728
68. He HP, Huang XJ, Chen LQ. Effective way to detect the secondary phase in Sr-doped $LaInO_3$. J Phys Chem Solids. 2001;62:701–9. doi:10.1016/S0022-3697(00)00220-1
69. Sood K, Singh K, Pandey OP. Studies on Sr substituted lanthanum indate as mixed ionic conductor. J Mater Sci. 2012;47:4520–9. doi:10.1007/s10853-012-6297-2

70. Kim HL, et al. Electrical conduction behavior of BaO-doped $LaInO_3$ perovskite oxide. Japanese J Appl Physics. 2006;45:872–4. doi:10.1143/JJAP.45.872
71. Yoon M-Y, et al. Molecular dynamics simulation of the effect of dopant distribution homogeneity on the oxide ion conductivity of Ba-doped $LaInO_3$. J Power Sources. 2014;248:1085–9. doi:10.1016/j.jpowsour.2013.10.054
72. Byeon D-S, et al. Oxide ion diffusion in Ba-doped LaInO3 perovskite: A molecular dynamics study. J Power Sources. 2013;222:282–7. doi:10.1016/j.jpowsour.2012.08.091
73. Kim H-L, et al. Oxygen ion conduction in barium doped $LaInO_3$ perovskite oxides. J Power Sources. 2014;267:723–30. doi:10.1016/j.jpowsour.2014.06.006
74. Kim H-L, Kim S, Lee H-L. Phase Formation and Proton Conduction of $La_{0.6}Ba_{0.4}In_{1-y}M_yO_{3-\delta}$ (M= Ga^{3+}, Sc^{3+}, Yb^{3+}) System. J Korean Ceram Soc. 2002;39:610–5. doi:10.4191/kcers.2002.39.6.610
75. Hwang K-J, et al. The Effect of Co-Doping at the A-Site on the Structure and Oxide Ion Conductivity in $(Ba_{0.5-x}Sr_x)La_{0.5}InO_{3-\delta}$: A Molecular Dynamics Study. Materials (Basel). 2019;12. doi:10.3390/ma12223739
76. Lee KH, et al. Phase formation and electrical conductivity of Ba-doped $LaScO_3$. Japanese J Appl Physics. 2005;44:5025–9. doi:10.1143/JJAP.44.5025
77. Kim S, Lee KH, Lee HL. Proton conduction in $La_{0.6}Ba_{0.4}ScO_{2.8}$ cubic perovskite. Solid State Ionics. 2001;144:109–15. doi:10.1016/S0167-2738(01)00887-6
78. Kato H, et al. Electrical conductivity of Al-doped $La_{1-x}Sr_xScO_3$ perovskite-type oxides as electrolyte materials for low-temperature SOFC. Solid State Ionics. 2003;159:217–22. doi:10.1016/S0167-2738(03)00101-2
79. Kumar S, et al. Study of structural, dielectric, optical properties and electronic structure of Cr-doped $LaInO_3$ perovskite nanoparticles. Mater Charact. 2017;131:108–15. doi:10.1016/j.matchar.2017.07.001
80. Nishiyama S, Kimura M, Hattori T. P-Type Electrical Conduction of $LaInO_3$ Based Ceramics and Calculation of its Density of States. Key Eng Mater. 2001;216:65–8. doi:10.4028/www.scientific.net/KEM.216.65
81. Egorova AV, et al. Oxygen ionic transport in $LaInO_3$ and $LaIn_{0.5}Zn_{0.5}O_{2.75}$ perovskites: Theory and experiment. Solid State Ionics. 2021;372:115790. doi:10.1016/j.ssi.2021.115790
82. Belova KG, et al. Electrical Properties of Co-doped $LaInO_3$ Perovskite. Russ J Inorg Chem. 2024. doi:10.1134/S0036023623602763
83. Thangadurai V, Weppner W. Synthesis and Electrical Properties of K- and Pr-Substituted $LaGaO_3$ and $LaInO_3$ Perovskites. J Electrochem Soc. 2001;148:A1294. doi:10.1149/1.1414286
84. Okuyama Y, et al. Proton Conduction and Incorporation into $La_{1-x}Ba_xYb_{0.5}In_{0.5}O_{3-\delta}$. Mater Trans. 2018;59:14–8. doi:10.2320/matertrans.MB201701
85. Nomura K, et al. Proton conduction in $(La_{0.9}Sr_{0.1})M^{III}O_{3-\delta}$ (M^{III}=Sc, In, and Lu) perovskites. Solid State Ionics. 2002;154–155:647–52. doi:10.1016/S0167-2738(02)00512-X
86. Animitsa I, et al. Incorporation of water in strontium tantalates with perovskite-related structure. Solid State Ionics. 2001;145:357–64. doi:10.1016/S0167-2738(01)00931-6
87. Uritsky MZ, Tsidilkovski VI. Proton transport in doped yttrium oxide. Monte-Carlo simulation. Russ J Electrochem. 2012;48:917–21. doi:10.1134/S1023193512090145
88. Putilov LP, Tsidilkovski VI. Impact of bound ionic defects on the hydration of acceptor-doped proton-conducting perovskites. Phys Chem Chem Phys. 2019;21:6391–406. doi:C8CP07745B
89. Hong SJ, Virkar A V. Lattice Parameters and Densities of Rare-Earth Oxide Doped Ceria Electrolytes. J Am Ceram Soc. 1995;78:433–9. doi:10.1111/j.1151-2916.1995.tb08820.x
90. Marrocchelli D, et al. Understanding Chemical Expansion in Non-Stoichiometric Oxides: Ceria and Zirconia Case Studies. Adv Funct Mater. 2012;22:1958–65. doi:10.1002/adfm.201102648
91. Hirata Y, et al. Synthesis and electrical conductivity of $(La_{1-x}Sr_x)(Al_{1-y}Mg_y)O_{3-\delta}$ perovskite solid solution. J Asian Ceram Soc. 2014;2:176–84. doi:10.1016/j.jascer.2014.03.005
92. Chatzichristodoulou C, et al. Size of oxide vacancies in fluorite and perovskite structured oxides. J Electroceramics. 2015;34:100–7. doi:10.1007/s10832-014-9916-2
93. Marrocchelli D, Perry NH, Bishop SR. Understanding chemical expansion in perovskite-structured oxides. Phys Chem Chem Phys. 2015;17:10028–39. doi:10.1039/C4CP05885B
94. Zhang J, et al. Tuning oxygen vacancies in epitaxial $LaInO_3$ films for ultraviolet photodetection. Opt Lett. 2022;47:5044. doi:10.1364/ol.470587
95. Rogers DB, Honig JM, Goodenough JB. The electrical properties and band structure of doped $LaInO_3$. Mater Res Bull. 1967;2:223–30. doi:10.1016/0025-5408(67)90061-X
96. Galazka Z, et al. Melt Growth and Physical Properties of Bulk $LaInO_3$ Single Crystals. Phys Status Solidi. 2021;218:2100016. doi:10.1002/pssa.202100016
97. Jang DH, et al. Single crystal growth and optical properties of a transparent perovskite oxide $LaInO_3$. J Appl Phys. 2017;121:125109. doi:10.1063/1.4977863
98. Kilner JA, Brook RJ. A study of oxygen ion conductivity in doped non-stoichiometric oxides. Solid State Ionics. 1982;6:237–52. doi:10.1016/0167-2738(82)90045-5
99. Zheng Y-S, et al. Electronic Origin of Oxygen Transport Behavior in La-Based Perovskites: A Density Functional Theory Study. J Phys Chem C. 2019;123:275–90. doi:10.1021/acs.jpcc.8b11249
100. Egorova AV., et al. Ionic (O^{2-} and H^+) Transport in Oxygen-Deficient Perovskites $La_2Me^{+3}ZnO_{5.5}$. Russ J Electrochem. 2023;59:276–83. doi:S1023193523040055
101. Codorniu-Hernández E, Kusalik PG. Probing the mechanisms of proton transfer in liquid water. Proc Natl Acad Sci. 2013;110:13697–8. doi:10.1073/pnas.1312350110
102. Pauliukaite R, Juodkazytė J, Ramanauskas R. Theodor von Grotthuss' Contribution to Electrochemistry. Electrochim Acta. 2017;236:28–32. doi:10.1016/j.electacta.2017.03.128
103. Mogensen M, et al. Factors controlling the oxide ion conductivity of fluorite and perovskite structured oxides. Solid State Ionics. 2004;174:279–86. doi:10.1016/j.ssi.2004.07.036
104. Zvonareva IA, Medvedev DA. Proton-conducting barium stannate for high-temperature purposes: A brief review. J Eur Ceram Soc. 2023;43:198–207. doi:10.1016/j.jeurceramsoc.2022.10.049
105. Lesnichyova AS, et al. Proton conductivity and mobility in Sr-doped $LaScO_3$ perovskites. Ceram Int. 2021;47:6105–13. doi:10.1016/j.ceramint.2020.10.189
106. Okuyama Y, et al. Proton transport properties of $La_{0.9}M_{0.1}YbO_{3-\delta}$ (M=Ba, Sr, Ca, Mg). Electrochim Acta. 2013;95:54–9. doi:10.1016/j.electacta.2013.01.156
107. Nguyen TL, et al. Hashimoto T. The effect of oxygen vacancy on the oxide ion mobility in $LaAlO_3$-based oxides. Solid State Ionics. 2000;130:229–41. doi:10.1016/S0167-2738(00)00640-8
108. Lerch M, Boysen H, Hansen T. High-temperature neutron scattering investigation of pure and doped lanthanum gallate. J Phys Chem Solids. 2001;62:445–55. doi:10.1016/S0022-3697(00)00078-0
109. Nomura K, Kageyama H. Neutron diffraction study of $LaScO_3$-based proton conductor. Solid State Ionics. 2014;262:841–4. doi:10.1016/j.ssi.2013.09.018
110. Stroeva AY, et al. Effect of scandium sublattice defectiveness on ion and hole transfer in $LaScO_3$-based proton-conducting oxides. Russ J Electrochem. 2011;47:264–74. doi:10.1134/S102319351103013X
111. Stroeva AY, et al. Phase composition and conductivity of $La_{1-x}Sr_xScO_{3-\alpha}$ (x = 0.01-0.20) Under oxidative conditions. Russ J Electrochem. 2012;48:509–17. doi:10.1134/S1023193512050114
112. Farlenkov AS, et al. Local disorder and water uptake in $La_{1-x}Sr_xScO_{3-\delta}$. Solid State Ionics. 2017;306:82–8. doi:10.1016/j.ssi.2017.04.018
113. Yukhno EK, et al. Physical and chemical properties of $LaInO_3$-

based phosphors doped with Dy^{3+}, Ho^{3+}, Sb^{3+} ions. Proceedings of the National Academy of Sciences of Belarus, Chemical series. 2017;4:31–7. Russian.

114. Inaba H, Hayashi H, Suzuki M. Structural phase transition of perovskite oxides $LaMO_3$ and $La_{0.9}Sr_{0.1}MO_3$ with different size of B-site ions. Solid State Ionics. 2001;144:99–108. doi:10.1016/S0167-2738(01)00904-3
115. da Silva CA, de Miranda PE V. Synthesis of $LaAlO_3$ based materials for potential use as methane-fueled solid oxide fuel cell anodes. Int J Hydrogen Energy. 2015;40:10002–15. doi:10.1016/j.ijhydene.2015.06.019
116. Lesnichyova A, et al. Water uptake and transport properties of $La_{1-x}Ca_xScO_{3-\alpha}$ proton-conducting oxides. Mater (Basel). 2019;12. doi:10.3390/ma12142219
117. Liu L. et al. Preparation, sinterability, electrical transport and thermal expansion of perovskite-type $La_{0.8}Ca_{0.2}CrO_3$ composites. Appl Sci. 2020;10:4634. doi:10.3390/app10134634
118. Tietz F. Thermal expansion of SOFC materials. Ionics (Kiel). 1999;5:129–39. doi:10.1007/BF02375916